Trajectory Analysis of Radiative Heating for Planetary Missions with Aerobraking of Spacecraft

Gene P. Menees*
NASA Ames Research Center, Moffett Field, California

Predictions of nonequilibrium and equilibrium radiative heating are obtained for the Titan aerocapture and two near-Earth aeroassisted orbital transfer vehicle (AOTV) missions. The Titan results include both the stagnation region and aft end of the fore cone of the conceptual aerocapture vehicle configuration for a range of entry parameters encompassing those of proposed mission profiles. The near-Earth AOTV results include orbit transfer between possible space station locations at geosynchronous and libration center L5 (a null point of the Earth-moon gravitational field overlap) orbits and equatorial and polar low Earth orbits, respectively. Several conceptual AOTV shapes, having a wide range of ballistic coefficients that simulate a variety of mission scenarios, are analyzed for each case. For both missions, results generally show that nonequilibrium is enhanced over equilibrium radiative heating and generally exceeds convective heating. Nonequilibrium radiative heating is thus an important factor in the design of thermal protection systems for Titan aerocapture and near-Earth AOTV missions and possibly for other future aeroassisted planetary missions. For Titan aerocapture, the nonequilibrium radiative heat flux can exceed several kilowatts per square centimeter, which is comparable to that of the Venus probe, and requires ablating-type materials to accommodate the heat shielding requirements. For near-Earth AOTV missions, the nonequilibrium flux dominates and is of such magnitude that nonrigid AOTV concepts are impractical without major breakthroughs being made in flexible, reusable materials technology. For rigid AOTV concepts, however, generic thermal protection systems (by use of non-ablating materials) may possibly satisfy the bulk of mission requirements in cislunar space.

Nomenclature

A_{ref} = entry vehicle reference area
C_D = drag coefficient
H = altitude
L/D = lift-drag ratio
L_i = libration centers of Earth-moon system ($i=1,5$)
M = entry vehicle mass
q_c = convective heat flux
q_r = radiative heat flux
Q_T = total heat load over flight trajectory
R_B = entry vehicle base radius
R_N = entry vehicle nose radius
t = flight time for atmospheric entry altitude
V = flight velocity
β = ballistic coefficient, M/C_DA
γ = flight-path angle relative to local horizon

Subscripts

E = atmospheric entry condition
s = stagnation point
∞ = freestream condition

Introduction

RECENT studies[1-9] have shown the substantial improvement in performance gained by spacecraft using the aerodynamic drag generated during grazing passes through planetary atmospheres to expend energy in excess of that required when achieving closed orbits. The propulsion fuel mass saved by eliminating costly retropropulsive braking maneuvers makes possible missions that are otherwise impossible or impractical.

The aerobraking maneuver is possible for any atmosphere-bearing planet or satellite. Conceptual feasibility studies have been made for both inner and outer planetary missions. Future applications that have been emphasized include 1) use of Titan's atmosphere to brake an interplanetary cruise vehicle from a hyperbolic flyby trajectory into a closed planetary orbit from which exploratory probes are launched to Titan and Saturn and 2) use of the upper terrestrial atmosphere to modify Earth-orbital trajectories for the development of advanced space transportation systems. The aerothermal environments of these missions have been investigated[1-11] with the assumption of chemical and local thermodynamic equilibrium. More recent studies,[12,13] however, examined the question of chemical equilibrium and its significance to the radiative surface heating rates. It was shown in Ref. 12 that, for most of a typical flight regime, the chemical composition of the shock layer is significantly out of equilibrium over the conical portion of the Titan aerocapture vehicle. Furthermore, as a consequence of the nonequilibrium chemistry, it was demonstrated that the radiative emission in the inviscid region of the shock layer could be enhanced significantly over the equilibrium state. Similar results were found in Ref. 13, which showed the potential importance of nonequilibrium shock-layer chemistry to the heat shield design for near-Earth orbital transfer vehicle missions.

The purpose of the present study is to examine the influence of atmospheric entry trajectory parameters on the magnitude of the radiative heating rates for both the Titan aerocapture and near-Earth orbital transfer vehicle missions. The relative importance of the equilibrium and nonequilibrium radiative and convective heating rates is determined, as well as their significance in the design of the corresponding thermal protection systems.

Computational Method and Verification

Complete computational procedures for obtaining the present predictions of the nonequilibrium and equilibrium radiative emissions from a reacting gas mixture are given in

Presented as Paper 83-0407 at the AIAA 21st Aerospace Sciences Meeting, Reno, Nev., Jan. 10-13, 1983; received March 7, 1984; revision received July 2, 1984.

*Research Scientist. Member AIAA.

Ref. 13. The present author collaborated in the development of the radiative transport computer code and is principally responsible for the final version used for validation studies and subsequent research. In general, the procedure involves the numerical calculation of the chemical reactions for inviscid flow behind oblique shock waves at conditions simulating specified locations on entry vehicle configurations. The radiative transfer owing to the nonequilibrium chemistry is determined by accounting for the deviation from equilibrium of the electronic state populations, using state-of-the-art spectral physics. The present results represent the incident radiative flux at the boundary-layer edge, since the calculations concern only the inviscid region of the shock layer. The extent to which the thickness of the boundary layer truncates the radiative emission by cooling the shock-layer gases, and reduces the surface intensity by absorbing the radiative flux, is not known but is approximated by terminating the calculations at 0.2 μm. Experience with entry-body flowfields indicates that most of the radiative flux below this spectral frequency range is absorbed in the boundary layer. In addition, the present method does not account for low-density phenomena of upper atmosphere flight regimes. However, the method is applicable over the important heating range of the entry cases considered herein, since an examination of Knudsen numbers shows the flow to be in the continuum or pseudo continuum regime.

The present results could be verified only for Earth re-entry missions because the appropriate experimental data are limited. This issue is discussed in Ref. 13 where comparisons are made with pre-Apollo era shock-tube and ballistic range test data for blunt bodies at entry velocities spanning the mission range of Earth orbital, lunar return, and return from the near planets. The general conclusion from this analysis is that the present method can determine the radiative heating to within a factor of about two for hypervelocity flight in air. For the case of Titan aerocapture, however, no experimental data exist for radiative emission from a gas mixture corresponding to Titan's atmospheric model. Nevertheless, the accuracy of Earth re-entry predictions is considered applicable to Titan, since the estimated chemical composition of Titan's atmosphere is similar to that of air (being nitrogen-rich with a small fraction of argon).

Results and Discussion

Titan Aerocapture Mission

For the present work, Titan's atmospheric structure is that proposed by Appleby (in Ref. 7) and, to conform with other recent studies, the chemical composition is taken to be 89% N_2/8% Ar/3% CH_4 by volume. Complete results are given in Figs. 1-6. The conceptual configuration (Fig. 1) is a bent biconic with variable lift obtained by roll control modulation. Flight trajectories obtained for what are possibly the allowable range of entry parameters for velocity, inclination, drag coefficient, lift-drag ratio, and ballistic coefficient are given in Fig. 2. The altitude range for perigee location or maximum and minimum atmospheric penetration by the aerocapture vehicle is thus determined. The results should also span the extremes of the radiative heating range and, therefore, identify entry conditions that minimize design constraints on the thermal protection system. The calculations were performed for a vehicle mass of 2300 kg with the base area used for reference purposes. Complete details of the entry conditions corresponding to the various cases that identify the flight trajectories are given in Table 1.

The maximum atmospheric penetration is obtained for case 1, which has the maximum entry angle (−45 deg), maximum velocity (12 km/s), minimum drag coefficient (~0.5), and minimum lift-drag ratio (~1.0). These conditions provide a ballistic coefficient of 800 kg/m^2, which is currently considered the most favorable. The entry velocity of 12 km/s is also considered most likely, since it is the most competitive with an all-propulsive system. Case 2 represents a simple aerodynamic maneuver imposed on case 1. Maneuvering is typically performed after the perigee location in the flight trajectory in order to correct for dispersions in the guidance, navigation, and control errors or to achieve a lower atmospheric exit velocity than that provided by a non-maneuvering trajectory. The minimum atmospheric penetration is shown by case 3, which is obtained with the minimum entry angle of −25 deg and the maximum values of the drag coefficient (~1.0) and lift-drag ratio (~2.0). There is a difference of about 100 km between the maximum and minimum penetration depths or perigee altitudes. Case 4 was obtained for the same conditions as case 3 with the exception of the entry velocity of 8 km/s, which is the minimum considered for Titan. About the same perigee altitude is obtained as for case 3 since the lift and ballistic coefficients are the same.

Also shown in Fig. 2 is the extent of the aerosol layer in Titan's atmosphere. It results from the condensation of hydrocarbon chemical species and extends ~100-280 km (communicated by J.N. Cuzzi, NASA Ames Research Center, Oct. 1982). The liquid droplets that compose the aerosol layer are destructive to a heat shield in hypersonic flow.[14] Consequently, it is desirable to spend a minimum amount of flight time in this region. This is achieved by shallow entry angles, high values of the lift and drag coefficients, and elimination of aerodynamic maneuvering. These factors have a strong influence on the radiative heating, as will be shown subsequently. The aerosol erosion problem can also be alleviated by employing a melting ablator, such as silica phenolic.

The flight velocity histories corresponding to the various entry conditions are shown in Fig. 3. The greatest deceleration occurs for cases 1 and 2, which are the steepest entries and

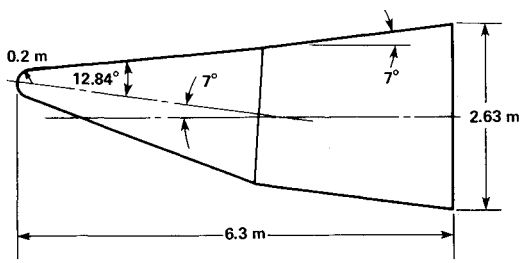

Fig. 1 Titan aerocapture vehicle configuration.

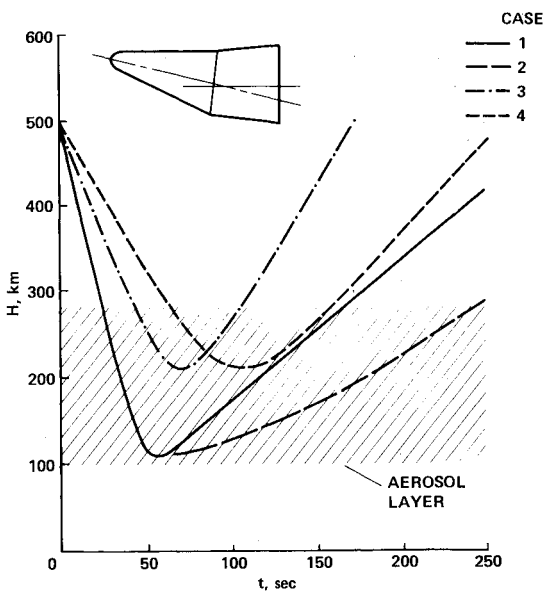

Fig. 2 Effect of entry parameters on flight trajectories for Titan aerocapture.

therefore penetrate to the denser regions of the atmosphere. In these cases, most of the entry velocity has been depleted by the time the perigee location is reached. However, the aerodynamic maneuvering in case 2 has an additional and significant effect in reducing the exit velocity. The atmospheric deceleration is progessively smaller for cases 3 and 4, because the shallower entry angle and lower velocity, respectively, result in flight through the upper, more rarefied regions of the atmosphere.

The predicted nonequilibrium and equilibrium radiative heat fluxes are compared in Fig. 4 over the range of the various flight trajectories. Results were obtained for two important locations on the aerocapture vehicle surface: the stagnation point (Fig. 4a) and the flank near the aft end of the fore cone (Fig. 4b). The equilibrium fluxes are overpredicted by a factor of about two in the present study, because all calculations are based on the nonequilibrium shock standoff distance. Accounting for this fact, the nonequilibrium results are considerably enhanced over those for equilibrium for all the entry conditions investigated at both vehicle locations. The stagnation point heat fluxes are much greater than those on the flank because of the higher shock-layer temperature caused by the greater angle of the bow-shock wave. The highest heating rates at either vehicle location are obtained for the deepest penetration into the atmosphere (cases 1 and 2) and the nonequilibrium rates exceed those for equilibrium over most of the flight trajectory range. The double peak in both the nonequilibrium and equilibrium distributions on the flank for cases 1 and 2 is not completely understood, but is believed to result from dissociation phenomena. The differences between cases 1 and 2 are not discernible because the aerodynamic maneuvering occurs after the perigee location. Beyond this flight time the velocity has decreased to such an extent that the shock-layer temperature falls below the level for important radiation emission. The shallow entry angle of case 3 causes the radiation to decrease substantially because of the rarefied density range of the upper atmosphere flight regime. However, the nonequilibrium rates become more dominant over the equilibrium case. The shallow entry combined with the low velocity of case 4 further reduces the heating rates and shows the nonequilibrium flux to be totally dominant over that for equilibrium, which is insignificant on the scales of Fig. 4. This illustrates the strong velocity-density dependence of the radiative flux and emphasizes the greater relative importance of the nonequilibrium state for the rarefied, upper atmosphere, hypersonic flight conditions typical of planetary entry.

The only source for comparison of the present predictions of radiative flux for the same Titan atmospheric model are the results of Moss.[11] These calculations were obtained for coupled, viscous, hypersonic flow with equilibrium chemistry over a blunt cone with a half-angle equivalent to the windward surface of the Titan aerocapture configuration at trim incidence. Results for both laminar and turbulent boundary-layer flows were obtained and found to have a negligible effect on the surface radiative heating rates. The present predictions of equilibrium radiative flux were compared with those of Moss at the same conditions in a proposed Titan flight trajectory near the peak heating point for the aforementioned vehicle locations. The present results are

Table 1 Entry parameters for Titan aerocapture trajectories[a]

Case	β	C_D	L/D	V_E, km/s	γ_E, deg
1	800	0.53	1.0	12	−45
2	800	0.53	Variable	12	−45
3	400	1.06	2.0	12	−25
4	400	1.06	2.0	8	−25

[a] $M = 2300$ kg, $A_{ref} = 5.43$ m^2, atmospheric composition 89% N_2 8% Ar 3% CH_4.

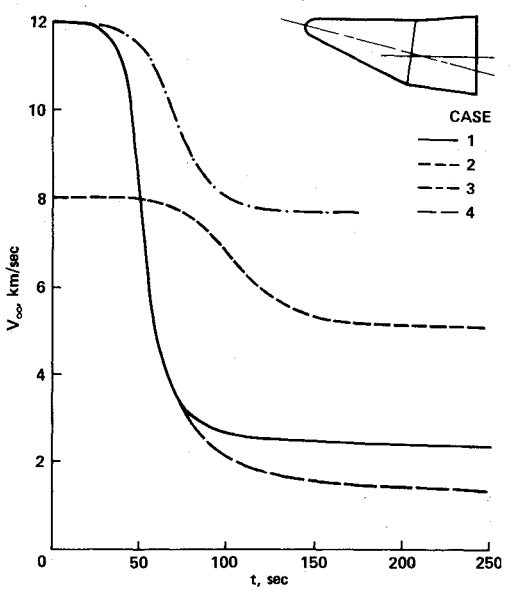

Fig. 3 Effect of entry parameters on flight velocities for Titan aerocapture.

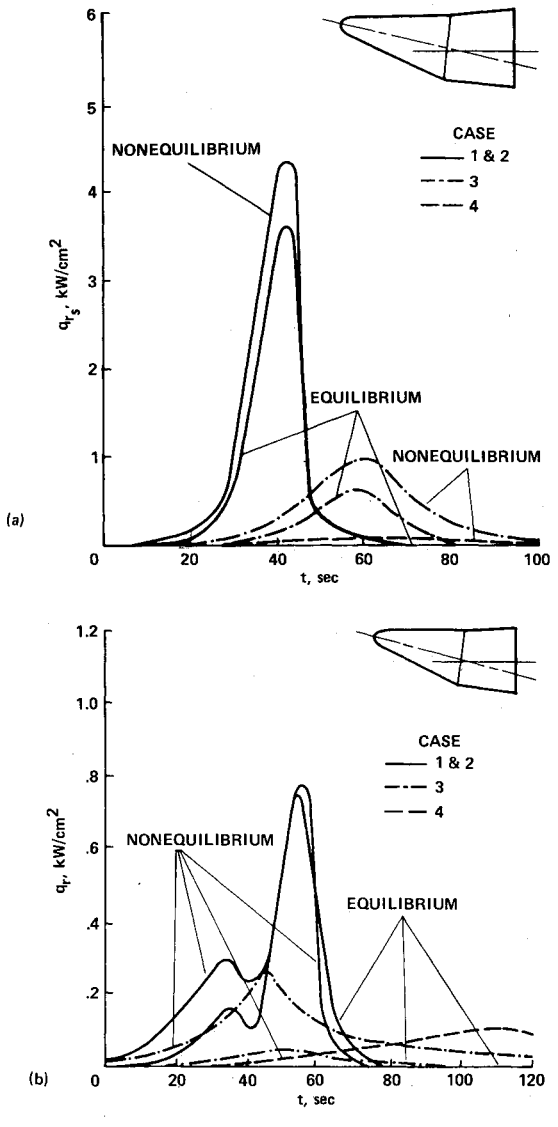

Fig. 4 Effect of entry parameters on radiative heating for Titan aerocapture: a) stagnation point; b) windward surface near aft end of fore cone.

typically higher at the stagnation point and lower on the flank than the results of Moss. These differences can be attributed to several factors that are not the same in the computational methods used to obtain the radiative flux. At the stagnation point, the radiative emission is from atoms only, since the higher temperature (~12,000 K) dissociates all species. The present method contributes to higher emission because of the greater detail in the line-by-line calculations for all atomic radiating species and is considered accurate since the oscillator strengths of atomic species are well know. In addition, the equilibrium chemistry calculations employed by Moss could produce significant differences, relative to the present method, in the stagnation region. This results from the polynomial curve fit for thermodynamic properties (enthalpy, specific heat, and free energy) required for the free-energy minimization technique. The Lewis curve fit used by Moss extends only to 6000 K and must be extrapolated to ~12,000 K in the stagnation region. This could cause errors at higher temperatures, since direct functions of temperature are used in the polynomial curve fit formulation. The present method is more accurate because thermodynamic properties are determined from partition functions, which are known for atomic species. At the flank location near the aft end of the fore cone, the radiative flux results primarily from molecular band continuum emission from N_2 and CN, as a consequence of the lower temperature regime (~6000-8000 K). The method used by Moss greatly overpredicts the radiative flux at this location because of the "smearing" approximation used for the molecular band continuum emission, which neglects the self-absorption of the line-by-line calculations of the present method. Another factor that causes the prediction of Moss to be higher on the flank results from the two-dimensional flowfield calculation of the equivalent blunt-cone approximation to the aerocapture vehicle configuration. This procedure causes higher temperatures at the boundary-layer edge, because the cooling of the flow on a body at large incidence resulting from expansion caused by three-dimensional cross-flow effects is neglected. Consequently, the high stagnation region temperatures are not sufficiently damped and are perpetuated far downstream on the vehicle flank. This overpredicts the radiative emission, which is a very strong exponential function of temperature, varying between the 10th and 20th powers. The present flat-plate-type approximations are considered more realistic in the flank region of the aerocapture vehicle at angle of attack, because the constant-flow properties across the shock layer simulate a cooling effect and provide lower temperatures.

The convective heating rates corresponding to the various flight trajectories are given in Fig. 5. The stagnation point results, shown in Fig. 5a, are the maximum convective rates on the vehicle surface and were obtained from the Fay-Riddell expression[15] modified for the atmospheric chemistry of Titan. They are in qualitative agreement with the results of Moss. The convective heating rates on the vehicle flank are given in Fig. 5b for both laminar and turbulent boundary-layer flows. These results were estimated from the calculations of Moss. The turbulent heating rates are greater, by as much as a factor of four, than those of the laminar case for most of the entry conditions, and are more than one-half the corresponding stagnation point values. The radiative heating rates exceed the convective rates only for cases 1 and 2 at the stagnation point. On the vehicle flank, the turbulent convective rates are substantially greater than the radiative rates. For the laminar condition, however, the radiative rates exceed the convective for cases 1 and 2 but are of the same order for cases 3 and 4. These differences between the radiative and convective rates may not be realistic, however, since the effects of ablation have not been considered. The entry conditions for proposed Titan missions are between cases 1 and 3. This will produce peak stagnation point heating rates of the order of several kilowatts per square centimeter, which are comparable to those of the Venus probe. An ablating heat shield material, such as carbon or silica phenolic, is necessary to accommodate heating rates of such magnitude. Previous studies have shown that the blowing of ablation products substantially reduces convective heating, thereby making radiation the dominant source of surface heating, even though some absorption occurs in the ablation layer. On the vehicle flank, the turbulent heating rates, which are of the order of 0.5 kW/cm^2, are valid because of the ablating stagnation region. This would not produce ablation but would cause pyrolysis of carbon phenolic, which would also result in a substantial reduction in the convective heating. Consequently, the nonequilirium radiative flux could be the major source of surface heating over the entire vehicle.

Table 2 Entry parameters and geometry of AOTV configurations[a]

Case	Shape	β, kg/m^2	C_D	R_N, m	R_N/R_B	A_{ref}, m^2
1	Ballute	22	1.06	12.20	–	468
2	Ballute	61	1.06	7.31	–	169
3	Hemisphere-cylinder	373	1.00	3.05	1.00	29
4	Sphere-cone	800	0.47	2.04	0.67	29

[a] $L/D=0$, $M=10.890$ kg (12 tons).

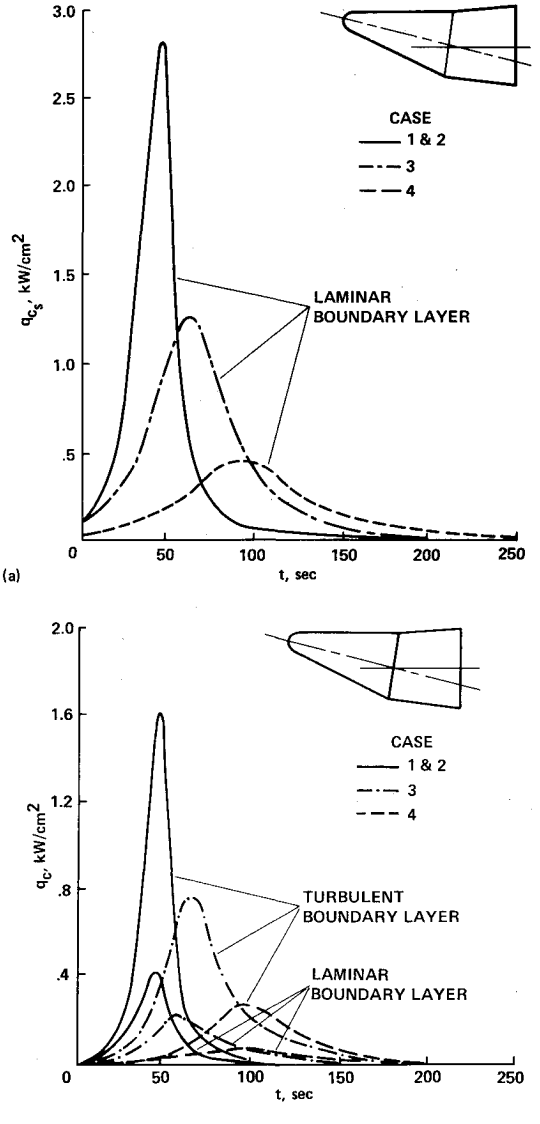

Fig. 5 Effect of entry parameters on convective heating for Titan aerocapture: a) stagnation point; b) estimated windward surface rates near aft end of fore cone.

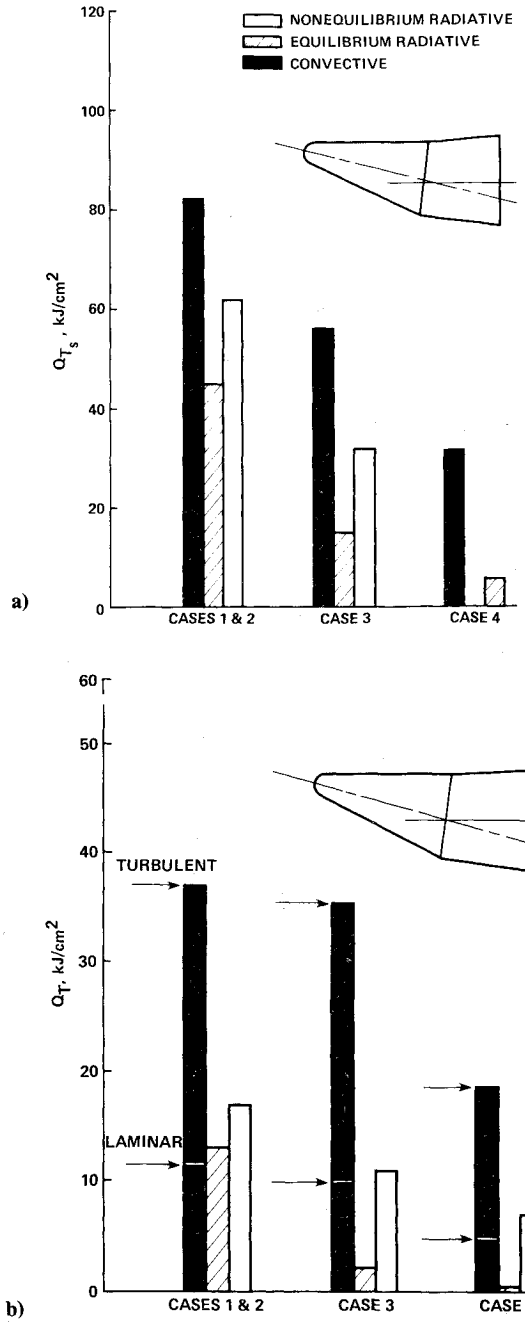

Fig. 6 Effect of entry parameters on total heat loads over flight trajectories for Titan aerocapture: a) stagnation point; b) windward surface near aft end of fore cone.

The total surface heat loads over the range of the various trajectories are given in Fig. 6. These results show the dominance of the convective heating in both the stagnation and flank regions, which is partly a result of the generally longer duration of the convective heating pulse in the flight trajectory. The relative importance of the nonequilibrium radiative heating is again emphasized when the substantial effects of ablation in reducing convective heating are accounted for. The magnitude of the total heat load can approach 50 kJ/cm^2, which is about one-third that for Jupiter entry. This will have an important impact on the feasibility of the Titan aerocapture mission, because the thermal protection system will require a significant fraction of the total vehicle mass. The design of a minimum-mass thermal protection system using state-of-the-art technology to meet all entry requirements will, therefore, not only enhance potential return benefits but may be crucial to the mission success.

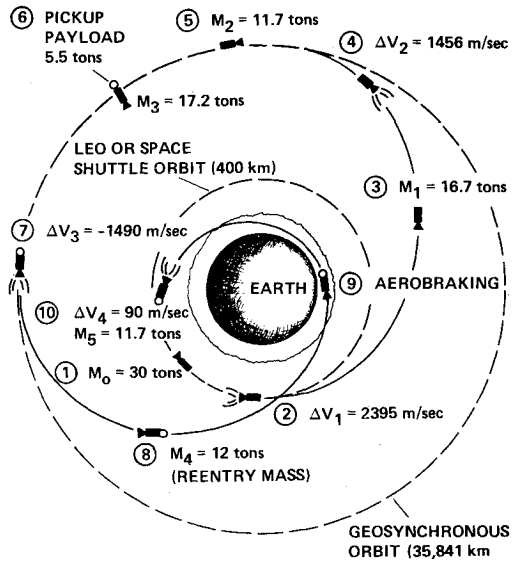

Fig. 7 Schematic of mission profile for a single-pass AOTV maneuvering between GEO and equatorial LEO (masses are computed assuming a specific impulse of 420 s).

Near-Earth Orbital Transfer Vehicle Missions

Geosynchronous to Equatorial Low-Earth Orbit

The location of a space station at geosynchronous orbit (GEO, 35,841 km altitude) is a future certainty because of its many scientific, commercial, and strategic applications. Consequently, low-cost orbital-change maneuvers between GEO and low Earth or Space Shuttle orbits (LEO, ~400 km altitude) for personnel and material transport will be a future requirement of high frequency. The advantages of aerobraking provide substantial savings in propulsion fuel mass for this mission. This is illustrated in Fig. 7 by the schematic of a typical mission profile for a single-pass, aerobraked orbital transfer vehicle (AOTV) maneuvering between GEO and equatorial LEO. Multiple passes are possible and appropriate for unmanned missions for which turnaround time is unimportant, but a single pass is appropriate for manned missions. The constraints on the mission are a re-entry mass of 12 tons (to conform with other studies) and the use of a liquid rocket engine with a specific impulse of 420 s to make the AOTV reusable and refuelable. The mission scenario is as follows: 1) the AOTV with initial mass of 30 tons (the approximate capacity of Space Shuttle cargo bay) is inserted into equatorial LEO; 2) a propulsive thrust of 2395 m/s is required to transfer from the circular LEO to an elliptical orbit with apogee at GEO and perigee at LEO; 3) this consumes a propulsion fuel mass of about 45% of the initial AOTV mass; 4) a propulsive thrust of 1456 m/s is required to achieve the circular GEO from the elliptical transfer orbit; 5) this maneuver consumes an additional 30% of the AOTV mass; 6) a payload of 5.5 tons is picked up for transfer to LEO so that a re-entry mass of 12 tons will be obtained subsequently; 7) a retropropulsive thrust of 1490 m/s is required for transfer to an elliptical orbit with perigee in Earth's atmosphere to take advantage of aerodynamic braking; 8) this maneuver expends 30% of the remaining AOTV mass in fuel and provides the desired re-entry mass of 12 tons; 9) aerodynamic braking occurs with the AOTV, achieving a new elliptical orbit with apogee at LEO; and 10) a final small propulsive thrust of 90 m/s is required for insertion into LEO, which burns a fuel mass of only 2.5%. Thus, aerobraking conserves essentially all of the fuel mass that would be required for return to LEO using all-propulsive maneuvers, which is about 45% of the AOTV mass (the difference between propulsive thrust for steps 2 and 10).

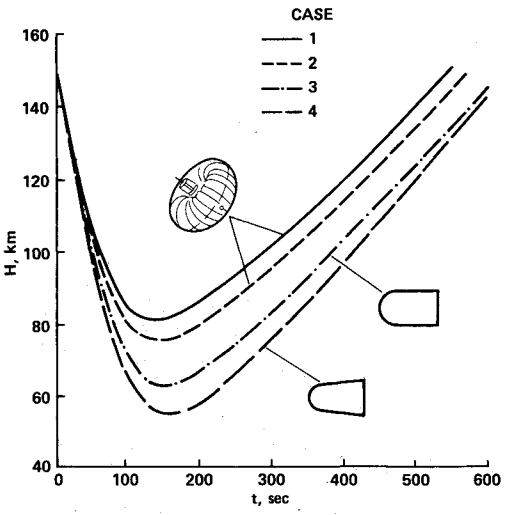

Fig. 8 Effect of entry parameters on AOTV flight trajectories for a single-pass mission from GEO to equatorial LEO.

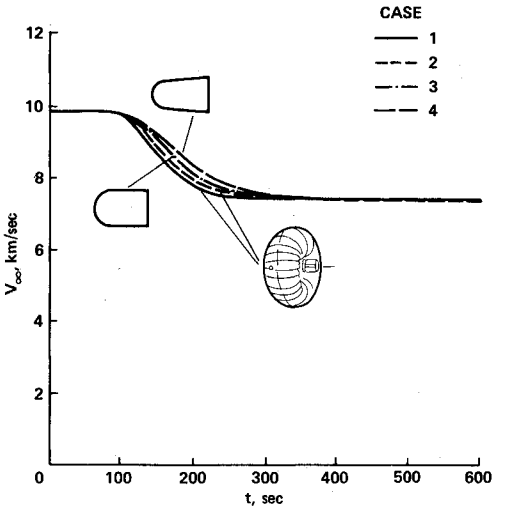

Fig. 9 Effect of entry parameters on AOTV flight velocities for a single-pass mission from GEO to equatorial LEO.

The entry trajectories for several AOTV configurations maneuvering between GEO and equatorial LEO are shown in Fig. 8. Because the design of AOTVs is still in the conceptual stage, nonlifting shapes having a wide range of ballistic coefficients are analyzed to determine the effect of atmospheric penetration, or perigee location, on the radiative and convective heating rates. This effect was shown to be substantial by the Titan results, since both heating rates are strong functions of velocity and density. In turn, velocity is a strong function of density because the vehicle deceleration is determined by the atmospheric density distribution, which varies exponentially with altitude. Complete details of the entry configurations are given in Table 2. Two of the shapes are bullutes of different diameters (cases 1 and 2). The ballutes are inflatable balloon-like structures that surround the AOTV during atmospheric entry and serve as a parachute-type drag device; they are deflated after the aerobraking maneuver is completed. The other two shapes are a hemisphere cylinder and blunt cone (cases 3 and 4, respectively) with base diameters close to that of the Space Shuttle cargo bay. The perigee altitudes shown in Fig. 8 are distributed in accordance with the ballistic coefficients of the various shapes. About 25 km separate the extremes, with the minimum penetration occurring for the large ballute and the maximum for the blunt cone. These shapes have a tremendous spread in ballistic coefficients, which are 22 and 800 kg/m^2, respectively. The velocity histories are shown in Fig. 9 and, as expected, the large ballute has the minimum deceleration and the blunt cone the maximum. All of the shapes have the same atmospheric entry and exit velocities because of the common vehicle mass (12 tons) and orbital-change requirements.

The radiative heating rate distributions over the flight trajectories are given in Fig. 10 for the stagnation point, because this location provides the maximum values on the body surface. For the ballutes, however, there is no physical stagnation point because, when inflated, the ballute is designed to surround the AOTV. The location selected for analysis is somewhat downstream of the geometric stagnation point, but is considered most critical to radiative heating in the shock layer. The ballistic coefficient, which is primarily a function of the configuration geometry since all cases have the same mass, is seen to have a tremendous effect on the magnitude of radiative heating. In addition, the nonequilibrium rates are greatly enhanced over those for equilibrium over the range of the flight trajectories. This effect is largest in the upper, more rarefied regions of the atmosphere and increases with perigee altitude, since these conditions provide the long relaxation times that make nonequilibrium effects important. The peak nonequilibrium

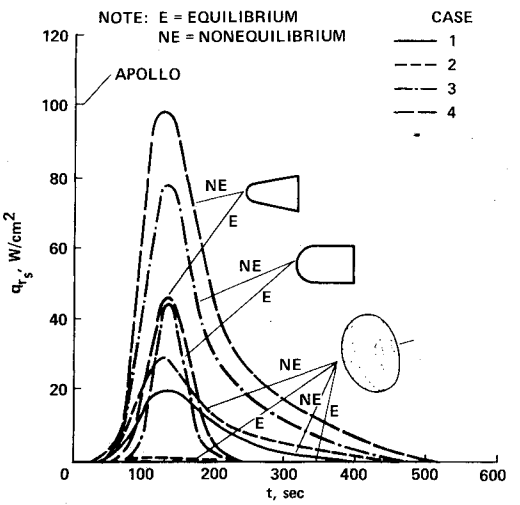

Fig. 10 Effect of entry parameters on AOTV radiative heating near stagnation point for a single-pass mission from GEO to equatorial LEO.

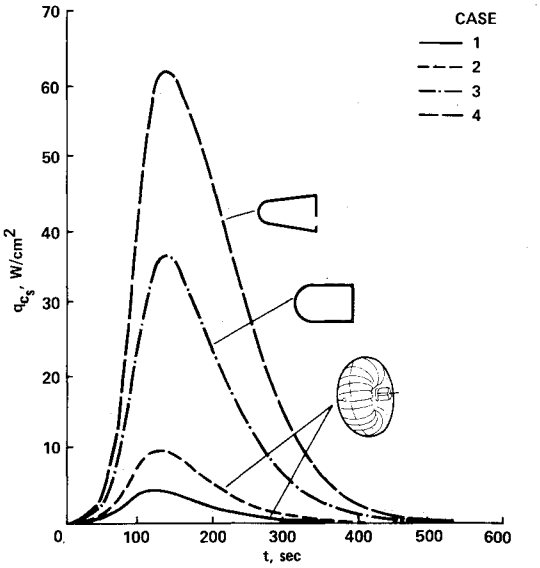

Fig. 11 Effect of entry parameters on AOTV stagnation point convective heating for a single-pass mission from GEO to equatorial LEO.

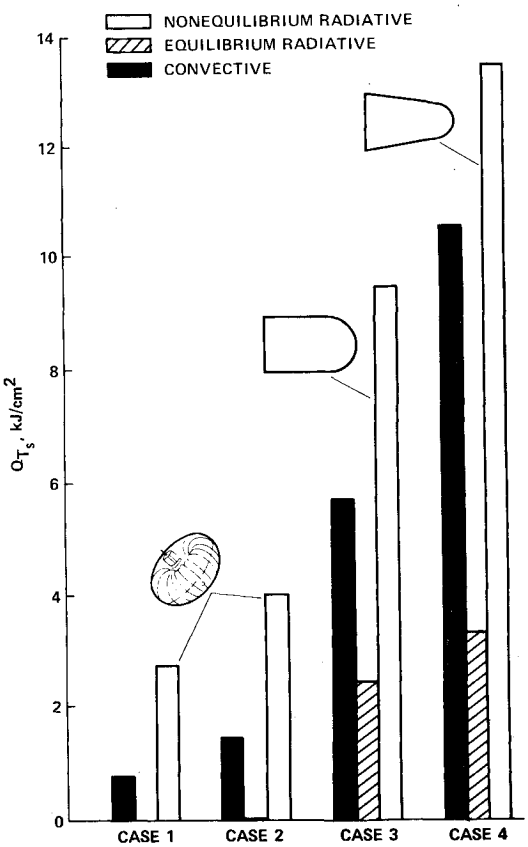

Fig. 12 Effect of entry parameters on AOTV total heat loads over flight trajectories for a single-pass mission from GEO to equatorial LEO.

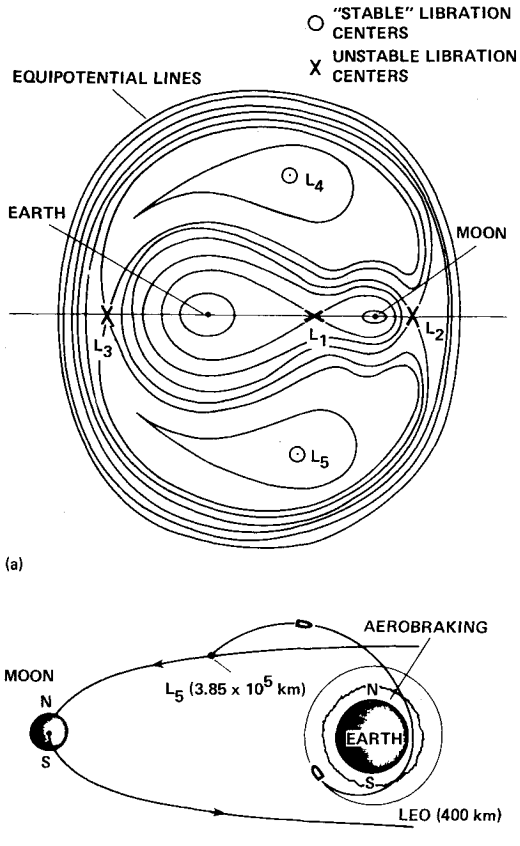

Fig. 13 Illustration of a hypothetical single-pass AOTV mission from libration center L5 to polar LEO: a) location of libration centers and equipotential lines for Earth-moon system (from Ref. 17); b) mission schematic.

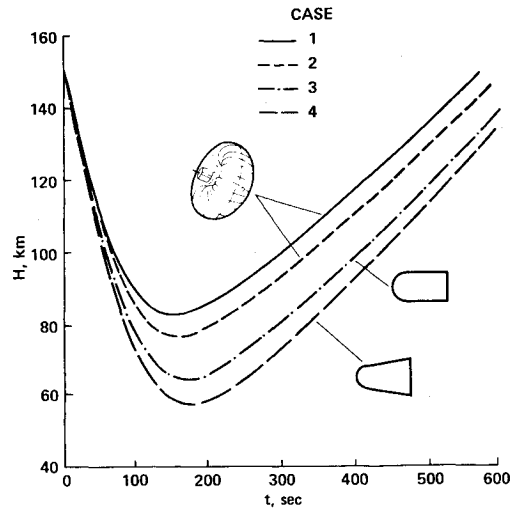

Fig. 14 Effect of entry parameters on AOTV flight trajectories for a single-pass mission from libration center L5 to polar LEO.

radiative flux varies from about 20 W/cm^2 for the large ballute (case 1) to about 100 W/cm^2 for the blunt cone (case 4). Coincidentally, this is also about the same radiative heat transfer measured for the Apollo experiment, which is noted on Fig. 10. The corresponding convective heating rates over the flight trajectories are given in Fig. 11. These results were also determined from the Fay-Riddell relation.[15] Again, the significant effect of flight in the denser regions of the lower atmosphere on the magnitude of the heating rates is evident. The nonequilibrium radiative rates of Fig. 10 substantially exceed the convective rates over the major portion of the flight trajectories for all cases. This is further illustrated by the total heat loads over the various trajectories shown in Fig. 12. The nonequilibrium radiative heating is thus an important factor in the thermal protection system design.

The combined value of the maximum nonequilibrium radiative and convective heat fluxes of this study are of the order of 25-40 W/cm^2 for the ballute configurations. Flexible, reusable thermal protection materials do not exist that can withstand heating rates of this magnitude. Consequently, the ballute concepts must be considered impractical without major breakthroughs in advanced materials technology. For the rigid high-ballistic coefficient shapes, the peak value of the combined nonequilibrium and convective heat fluxes is about 200 W/cm^2 and that of the total heat loads about 25 kJ/cm^2. Heating of this magnitude can be accommodated by a relatively thin carbon heat shield. For a similar flight regime, Park[16] previously examined the effect of chemical ablation by oxygen on a carbon heat shield and found that a thickness of 1 mm would sustain a heat flux of about 200 W/cm^2. However, because of the oxygen erosion problem, a reflecting material such as silica may be desirable. The crucial factor in selecting and sizing the heat-shield material, however, is the question of reusability (i.e., the number of missions required before refurbishing). This issue is beyond the scope of this study, but is determined by the weight penalties that are tolerable for the heat shielding requirements before the benefits of aeroassist are counteracted.

Libration Center L5 to Polar Low Earth Orbit

A space station at this location may be a future possiblity because of the advantages for scientific observations and experiments and, perhaps, strategic applications. The null relative force environment resulting from the superimposed gravitational fields of the Earth-moon system theoretically suspends the space station in orbit with no energy penalty.

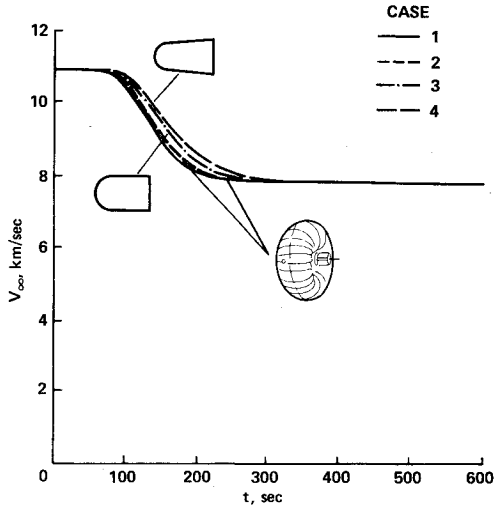

Fig. 15 Effect of entry parameters on AOTV flight velocities for a single-pass mission from libration center L5 to polar LEO.

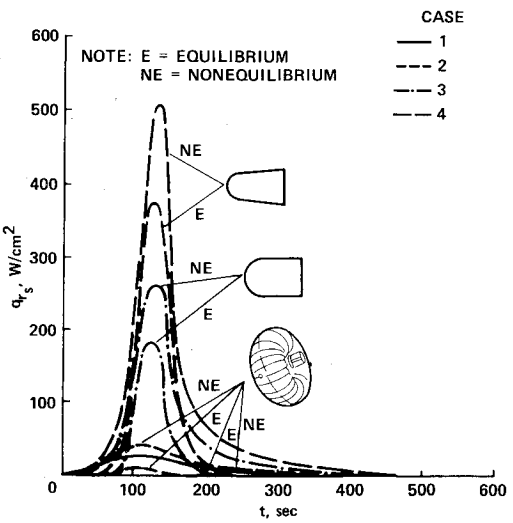

Fig. 16 Effect of entry parameters on AOTV radiative heating near stagnation point for a single-pass mission from libration center L5 to polar LEO.

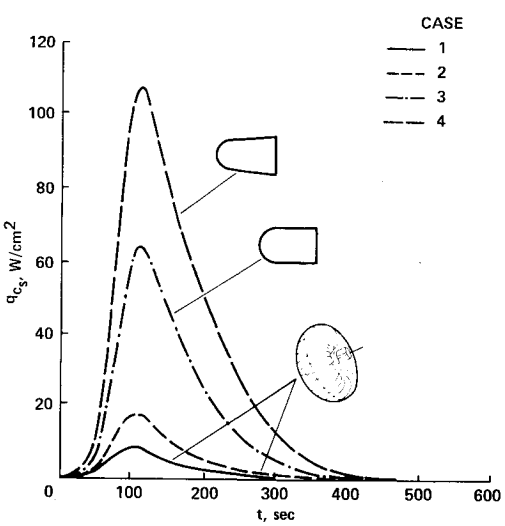

Fig. 17 Effect of entry parameters on AOTV stagnation point convective heating for a single-pass mission from libration center L5 to polar LEO.

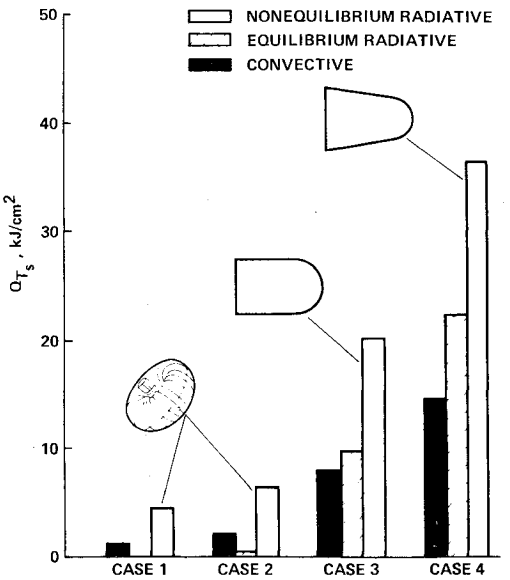

Fig. 18 Effect of entry parameters on AOTV total heat loads over flight trajectories for a single-pass mission from libration center L5 to polar LEO.

Consequently, negligible propulsive thrust is required for orbital transfers. This mission is analyzed because L5 is a stable libration center and the polar LEO gives the maximum entry velocity, which is about 1 km/s greater than the GEO to equatorial LEO case. The mission profile is illustrated in Fig. 13. The locations of the libration centers and equipotential lines in the Earth-moon system are discussed in Ref. 17 and are shown in Fig. 13a. A schematic of the orbit transfer maneuver is given in Fig. 13b. The orbital radius of L5 is equal to the lunar distance, because the stable libration centers are located at the apexes of the fore and aft equilateral triangles obtained using the Earth-moon axis as base points. The flight trajectories in Earth's atmosphere during the aerobraking maneuver are shown in Fig. 14 for the AOTV configurations described in Table 2. The perigee altitudes are lower than for the GEO to equatorial LEO mission (see Fig. 8) because of the steeper entry angle and higher entry velocity required for the orbit transfers. The flight velocity histories given in Fig. 15 show the greater atmospheric deceleration necessary to achieve the polar LEO (see Fig. 9). The higher exit velocity occurs because Earth's rotational velocity is not a factor in a polar entry. The radiative heating rates are given in Fig. 16 and are substantially greater in magnitude than for the GEO to equatorial LEO case, because of the higher flight velocities and deeper atmospheric penetrations. The nonequilibrium radiative rates are again greatly enhanced over the equilibrium case. For the extremes of the entry conditions corresponding to the large ballute and blunt cone, the peak nonequilibrium radiative flux is greater by factors of about two and five (see Fig. 10). The corresponding convective rates are given in Fig. 17 and are greatly exceeded by the nonequilibrium radiative rates. For peak heating conditions, the difference varies by factors of about two to four for the various configurations. The total heat loads over the flight trajectories are given in Fig. 18; again, the total domination of the nonequilibrium radiative heating for this mission is shown. The magnitudes of the combined nonequilibrium radiative and convective heat fluxes and the total heat loads are greater by a factor of about four than for the GEO to equatorial LEO mission. However, the previous discussion concerning thermal protection also generally applies here, indicating the possiblity of generic thermal protection systems that satisfy the bulk of mission requirements in cislunar space.

Conclusions

An analysis was made to determine the importance of radiative heating for the Titan aerocapture and two near-Earth aeroassisted missions. Calculations were obtained for a wise range of entry conditions encompassing those of many conceptual mission scenarios for both Titan and Earth. The results generally show that nonequilibrium is enhanced over equilibrium radiative heating and generally exceeds convective heating for most mission profiles. Consequently, non-equilibrium radiative heating is an important factor in the design of the corresponding thermal protection systems. For the Titan aerocapture mission, the peak heat fluxes and loads can be comparable to those for the Venus proble, which requires an ablating heat shield material, such as carbon or silica phenolic, for thermal protection. For near-Earth AOTV missions, the combined heating rates and loads are such that thermal protection is impossible for nonrigid inflatable concepts until advanced technology breakthroughs are made for flexible, reusable materials. For rigid AOTV concepts, however, generic heat shielding designs using nonablating materials (e.g., carbon, silica, or hot-metallic structures) may possibly satisfy the bulk of mission requirements in cislunar space.

References

[1]Cruz, M.I., "Aerocapture Vehicle Mission Design Concepts for Inner and Outer Planets," AIAA Paper 79-0893, May 1979.

[2]French, J.R. and Cruz, M.I., "Aerobraking and Aerocapture for Planetary Missions," *Astronautics and Aeronautics,* Feb. 1980, pp. 48-71.

[3]French, J.R. and McRonald, A.D., "Thermophysical and Systems Integration Considerations in Aerobraking Design," AIAA Paper 80-1492, July 1980.

[4]"Generic Aerocapture Atmospheric Entry Study—Final Report, Vol. 1," General Electric Re-Entry Systems Div., Doc. 80SDR2226, Oct. 24, 1980.

[5]Florence, D.E., "Aerothermodynamic Design Feasibility of a Generic Planetary Aerocapture/Aeromaneuver Vehicle," AIAA Paper 81-1127, June 1981.

[6]French, J.R., "Trends in Unmanned Planetary Entry Systems," AIAA Paper 81-1125, June 1981.

[7]Cruz, M.I., "Generic Aerocapture Technology Interchange Meeting Minutes, June 26, 1981, at Ames Research Center," Jet Propulsion Laboratory, Pasadena, Calif., Rept. IOM 312/81.8-568, July 14, 1981.

[8]Andrews, D.G. and Caluori, V.A., "Optimization of Aerobraked Orbital Transfer Vehicles," AIAA Paper 81-1126, June 1981.

[9]Walberg, G.D., "A Review of Aeroassisted Orbit Transfer," AIAA Paper 82-1378, Aug. 1982 (also, *Journal of Spacecraft and Rockets,* Vol. 22, Jan.-Feb. 1985, pp. 3-18, *Astronautics and Aeronautics,* Nov. 1983, pp. 36-43).

[10]Tiwari, S.N. and Chow, H., "Analysis of Aerothermodynamic Environment of a Titan Aerocapture Vehicle," AIAA Paper 81-1128, June 1981.

[11]Green, M.J. and Moss, J.N., "Aerothermodynamic Environment and Thermal Protection for a Titan Aerocapture Vehicle," AIAA Paper 84-1714, June 1984.

[12]Park, C., "Radiation Enhancement by Nonequilibrium during Flight through the Titan Atmosphere," AIAA Paper 82-0878, June 1982.

[13]Park, C., "Radiation Enhancement by Nonequilibrium in Earth's Atmosphere," *Journal of Spacecraft and Rockets,* Vol. 22, Jan.-Feb. 1985, pp. 27-36.

[14]Dunbar, L.E., Courtney, J.F., and McMillen, L.D., "Heating Augmentation in Erosive Hypersonic Environments," *AIAA Journal,* Vol. 13, July 1975, pp. 908-912.

[15]Fay, J.A. and Riddell, F.R., "Theory of Stagnation Point Heat Transfer in Dissociated Air," *Journal of the Aeronautical Sciences,* Vol. 25, Feb. 1958, pp. 73-85.

[16]Park, C., "Effects of Atomic Oxygen on Graphite Ablation," *AIAA Journal,* Vol. 14, Nov. 1976, pp. 1640-1642.

[17]Hornby, H. and Allen, W.H., "Mission to the Libration Centers," *Astronautics and Aeronautics,* July 1966, pp. 78-82.